

AN EXPERIMENTAL INVESTIGATION OF DEEP PENETRATION INTO POLYCARBONATE TARGETS

A. Weiss^{1,*}, A. Vizel¹ and D. Durban²

¹*Plasan Ltd., MP Merom Hagalil, 13870, Israel, e-mail: alonw@plasan.com*

²*Faculty of Aerospace Engineering, Technion, Haifa 32000, Israel*

Deep penetration experiments were conducted with polycarbonate targets at normal impact and within a striking velocity range of 600-900 m/sec. Three different projectile nose shapes (ogive, hemisphere and flat) were used in impact tests. Projectile penetration location, velocity and acceleration, were monitored using high-speed cameras for tracking the depth of penetration path and orientation. Data provided by tests was analyzed and compared to several theories available in current literature. We have examined in detail, for each nose profile, the dependence of resisting force on projectile velocity and sensitivity to projectile mass and contact surface friction. Best fit formulae for variation of penetration depth with striking velocity are suggested. Universal relations are constructed in non-dimensional variables with remarkable fit to experimental results. Contact is made with a recent study [8] on deep penetration of rigid projectiles with ogive head into polycarbonate targets. Finally, we have studied the predictive power of several deep penetration theories available in the literature, e.g. [11]-[12]. In particular, validity of cavitation model is assessed in context of Mises type plasticity constitutive response of polycarbonate.

INTRODUCTION

The earliest recorded studies on terminal ballistics date back to eighteenth century ideas by Euler and Robins [1] who argued that projectile resisting force remains constant during the penetration process. Later work by Poncelet (1829), Resal (1895) and Petry (1910) has paved the way [2] to modern penetration science and engineering in deriving velocity dependent formulae for resisting force. Comprehensive reviews on recent advances in deep penetration mechanics, including a discussion of the cavity expansion model, are available in references [3]-[6].

The present work reports experimental findings on deep penetration tests, at normal impact, with polycarbonate targets. Previous papers on deep penetration into polycarbonate targets include the experimental investigation on low speed cylindrical punch penetration [7], and the dynamic penetration study [8]. A related experimental study on design of transparent armor is presented in [9].

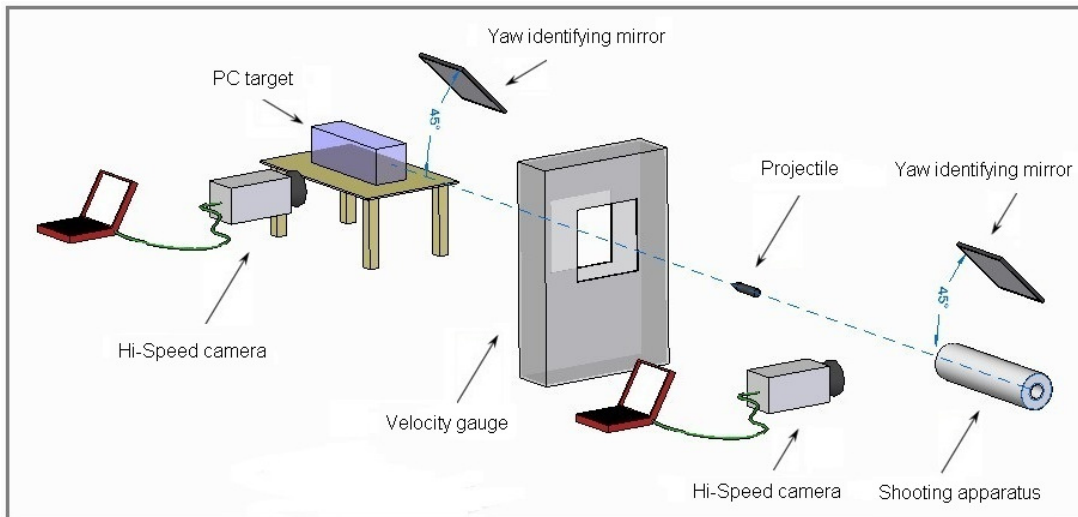


Figure 1. Schematics of the experimental set-up.

Deep penetration experiments were conducted on polycarbonate (PC) targets at normal impact and within a striking velocity range of 600-900 m/sec. Three different projectile nose shapes (ogive, hemisphere and flat) were used in a large number of impact tests. Projectile penetration history was monitored using high-speed cameras for tracking location, speed and acceleration, along the entire penetration path. Data provided by tests has been analyzed and compared to several theories available in current literature on penetration mechanics.

Here, due to limited available space, we shall outline just an illustrative part of the complete research [10]. We begin in the next section with a short description of the experimental set-up. A series of penetration tests with ogival head projectiles is detailed next and analyzed. Finally, contact with existing studies is made in the last section.

EXPERIMENTAL SET UP

The targets used in the present study were 100x100x T mm polycarbonate plates with thicknesses, T , varying from 300 to 500 mm, according to impact velocity. Two series of ballistic experiments were carried out (Series I and Series II). In Series I, the targets were dynamically loaded by 7.62 mm ogive-tip armor-piercing (AP) projectiles (with steel core, mass 9.91 gr, crh 6, core length 23.8 mm and shank length 32.4 mm) accelerated by a powder gun. The impact velocities ranged from 600 to 900 m/s. The shooting was perpendicular to the target; a single shot with a different velocity at each target. Two high-speed cameras (Phantom® V710, 50,000 FPS) continuously recorded the impact and penetration events. One camera was situated perpendicular to the bore of the shooting apparatus and the other was placed perpendicular to the trajectory of the projectile within the target. Two mirrors for yaw identification were located opposite each camera at an inclination of 45 degrees to the projectile's trajectory. A schematic presentation of the experimental set-up is shown in Fig. 1. In order to follow the path of the projectile within the target and to track the velocity and

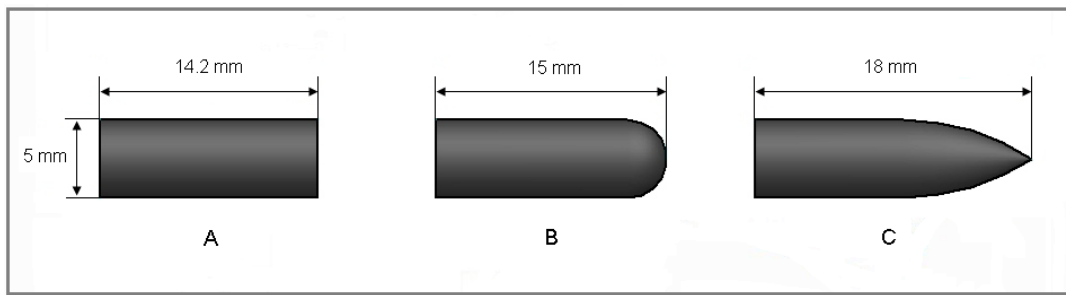


Figure 2. Three different Series II projectile nose shapes: A: flat. B: hemispherical. C: ogival (crh 3).

deceleration of the projectile inside the polycarbonate target, image processing of the high-speed photography was performed via the TEMA program.

In Series II, projectiles, developed and manufactured by Plasan Ltd., were made of hard steel with three different geometries of projectile nose shapes (ogival, hemispherical and flat), see Fig. 2. All three projectiles were of the same weight and diameter [mass 2 gr, diameter 5 mm]. The experimental configuration used in Series II was identical to the configuration used in Series I. In both series of experiments the projectiles were much more rigid than target material.

Fig. 3 displays the PC target after penetration of a 7.62 mm AP projectile. Due to the transparency of the PC target and the high sampling rate of the HS cameras, one can track the position, velocity and deceleration histories of the tip of the projectile along the penetration trajectory until complete stop inside the target. A noteworthy observation of this deep penetration process in polycarbonate is the significant recovery of the cavity along the trajectory, also observed in [8], which is evident from its smaller diameter compared to the projectile diameter, as shown in Fig. 4. While the projectile diameter is 7.62 mm, the post penetration tunnel diameter is approximately only 3.92 mm, nearly half of the projectile diameter. However, there is a wider zone of damaged plastic material around the projectile and the cavity which is visible even to the naked eye.

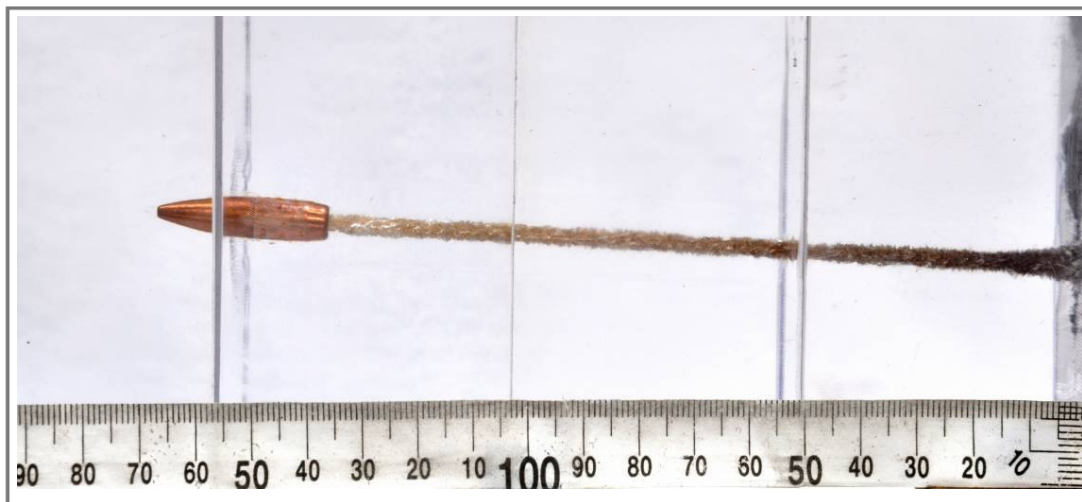


Figure 3. Deep penetration of 7.62 mm AP projectile in polycarbonate.

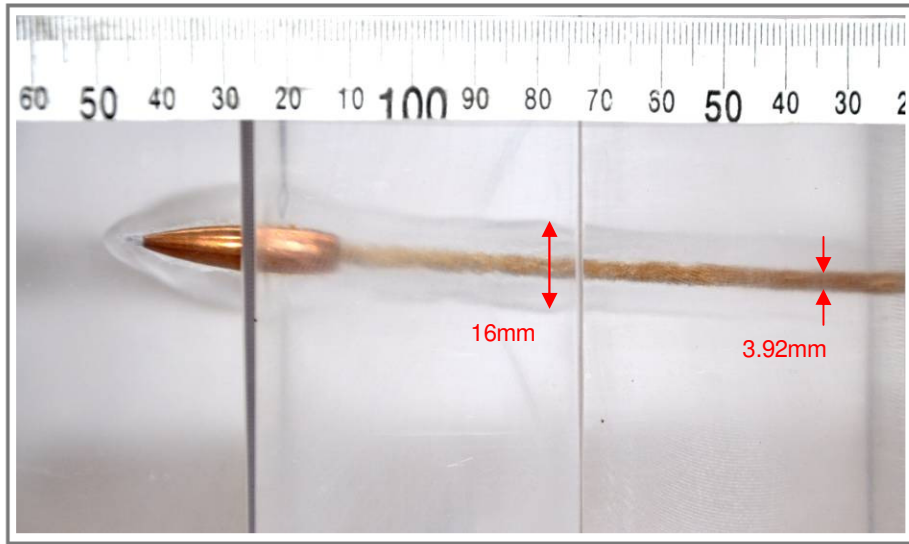


Figure 4. Crack zone in the polycarbonate target struck by a 7.62 mm AP projectile.

RESULTS AND DISCUSSION

Penetration trajectories monitored for seven normal impact tests are displayed in Fig. 5. Experiments were performed with identical ogive head projectiles (7.62 mm diameter and mass of 9.91 gr). We have tried to fit the experimental points with the simple polynomial approximation

$$x = V_s t - \frac{1}{2} x_2 t^2 + \frac{1}{3} x_3 t^3 \quad (1)$$

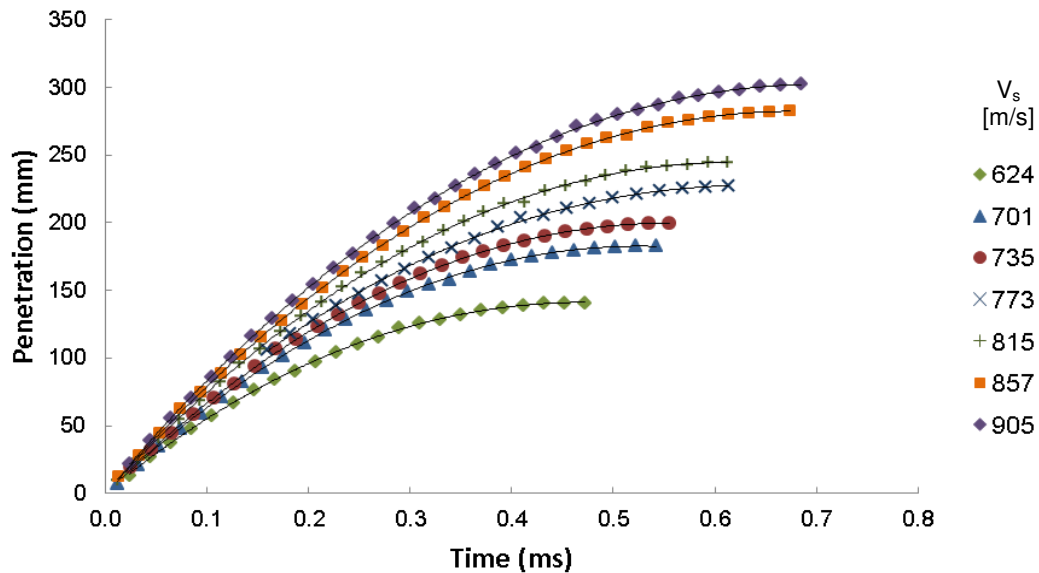


Figure 5. Penetration history of 7.62 mm AP into polycarbonate as function of time during normal penetration at impact velocities in the range of 624-905 m/s. Best fit curves are shown by full lines.

TABLE I. EXPERIMENTAL AND CALCULATED DATA (SERIES I).

V_s [m/s]	T [ms]	H [mm]	x_2 [$\times 10^3$ m/s ²]	x_3 [$\times 10^6$ m/s ³]	$V_s T/H$	V_s^2/H [$\times 10^3$ m/s ²]
624	0.467	141	1490	363	2.07	2.76
701	0.541	183	1370	69	2.07	2.69
735	0.553	200	1406	147	2.03	2.70
773	0.603	228	1502	468	2.04	2.62
815	0.610	245	1434	189	2.03	2.71
857	0.671	282	1374	165	2.04	2.60
905	0.679	302	1486	288	2.03	2.71

where x is the instantaneous location of the tip of the projectile, t denotes time, and (x_2, x_3) are disposable parameters to be determined. Impact velocity V_s is retained in (1) to comply with the initial condition $\dot{x}(0) = 0$. Evidently, the best fit values of parameters (x_2, x_3) , given in Table I, reveal excellent agreement (Fig.5) with experiments.

Furthermore, parameter (x_2) shows little sensitivity to impact velocity V_s . In fact, the average value of $\langle x_2 \rangle = 1437 \times 10^3 \text{ m/s}^2$ can be taken as the nominal, practically constant, value of x_2 with deviations of less than 5%. Parameter x_3 varies considerably with V_s yet the contribution of the cubic term in (1) remains small.

In that spirit we have examined the possibility that all seven curves of Fig. 5 admit a universal relation. To this end, relation (1) is rewritten in non-dimensional form as

$$\xi = \xi_1 \tau - \frac{1}{2} \xi_2 \tau^2 + \frac{1}{3} \xi_3 \tau^3 \quad (2)$$

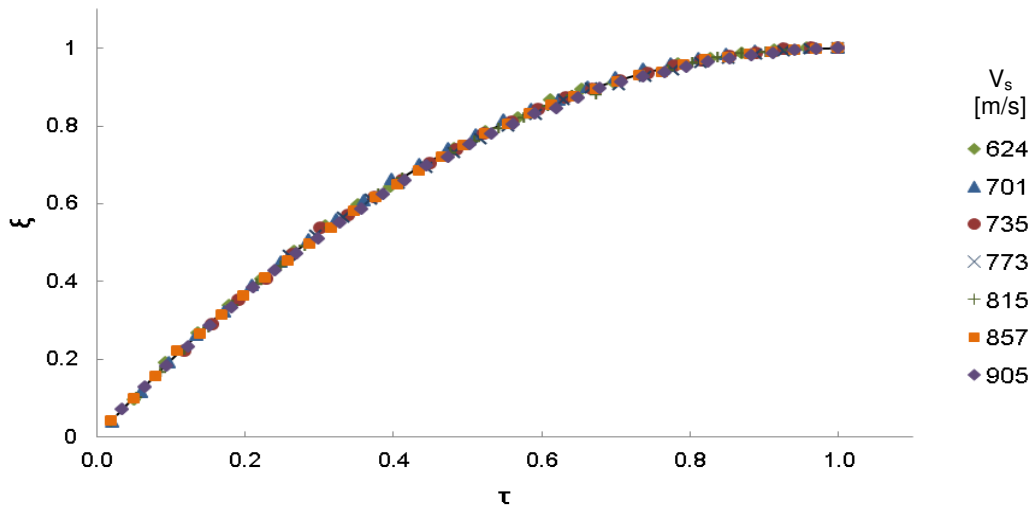


Figure 6. Normalized position ξ of 7.62 mm AP for polycarbonate as a function of normalized time, τ , during normal penetration at impact velocities in the range of 624-905 m/s. Best fit curves are shown by full lines.

where $\xi = x/H$ with H denoting final depth of penetration, $\tau = t/T$ with T as total penetration time, and coefficients (ξ_1, ξ_2, ξ_3) are to be determined. Imposing the three conditions, at impact and at terminal point,

$$\frac{d\xi}{d\tau}(\tau=0) = \frac{V_s T}{H} \quad \xi(\tau=1) = 1 \quad \frac{d\xi}{d\tau}(\tau=1) = 0 \quad (3)$$

and solving for (ξ_1, ξ_2, ξ_3) we find

$$\xi = E\tau - (2E-3)\tau^2 + (E-2)\tau^3 \quad \text{with} \quad E = \frac{V_s T}{H} \quad (4)$$

All seven trajectories of Fig. 5, shown again in Fig. 6 in the non-dimensional plane (ξ, τ) , clearly merge into a single curve. Indeed, with the best fit value of $E = 2.09$, determined numerically, relation (4) can be regarded as a universal relation (Fig. 6) describing all seven penetration histories with remarkable accuracy. In fact, calculated values of $V_s T/H$ for each of the seven tests are very close to the overall best fit value of 2.09, as shown in Table 1.

Turning to projectile velocity, we compare the universal relation, deduced from (4)

$$\frac{V}{H/T} = \frac{d\xi}{d\tau} = E - 2(2E-3)\tau + 3(E-2)\tau^2 \quad (5)$$

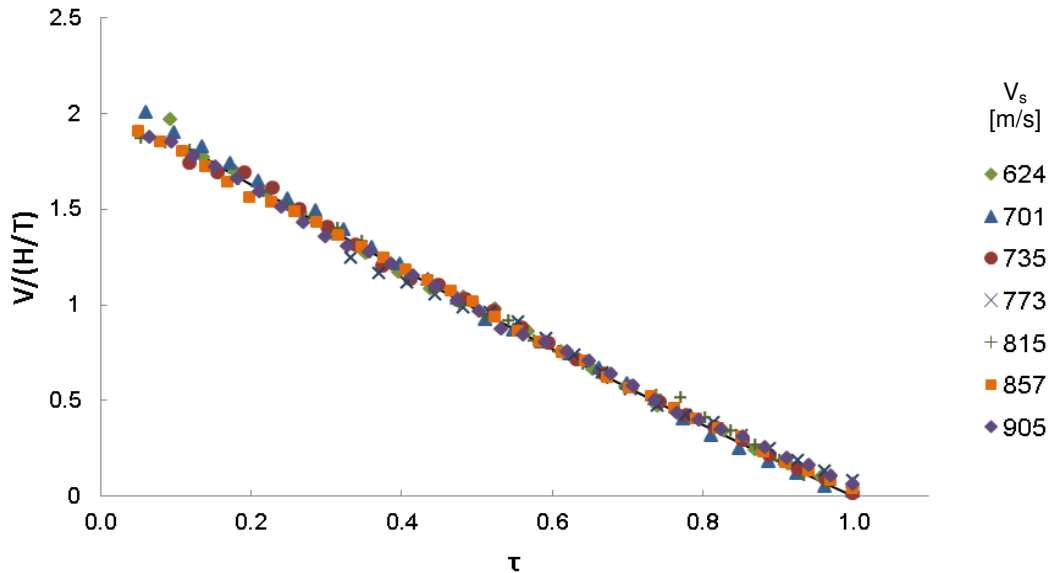


Figure 7. Normalized velocity $V/(H/T)$ of 7.62 mm AP for polycarbonate as a function of normalized time τ during normal penetration at impact velocities in the range of 624-905 m/s. Best fit curves are shown by full lines.

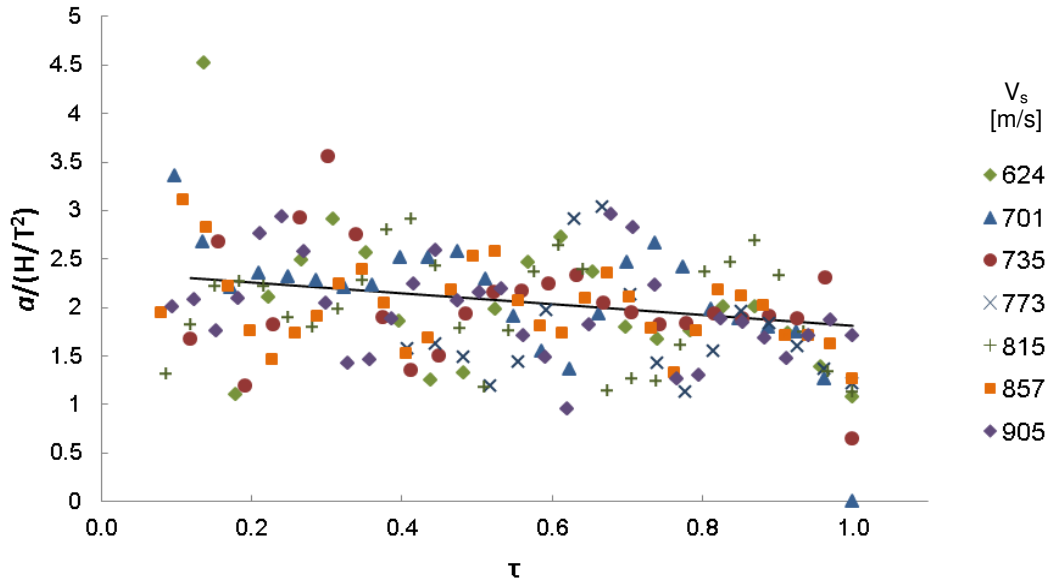


Figure 8. Normalized acceleration $a/(H/T^2)$ of 7.62 mm AP for polycarbonate as a function of normalized time τ during normal penetration at impact velocities in the range of 624-905 m/s. Best fit curves are shown by full lines.

where $V = dx/dt$ is projectile velocity, with the seven tests measurements of Fig. 7. Experimental velocity values have been measured during penetration process, for all seven cases. And agreement of collective data for $V/(H/T)$ with the proposed relation (5), when $E = 2.09$, is very good, though wave fluctuations are noticed.

Presence of travelling waves is apparent in acceleration records, compared in Fig. 8 with the prediction of our universal relation.

$$\frac{a}{H/T^2} = -\frac{d^2\xi}{d\tau^2} = 2(2E-3) - 6(E-2)\tau \quad (E = 2.09) \quad (6)$$

where we define the acceleration (a) in absolute value. Thus, to the first order, acceleration decreases linearly with time. It is worth noting, however, that the average value of the non-dimensional acceleration (6) is simply

$$\left\langle \frac{a}{H/T^2} \right\rangle = E \quad (7)$$

which is nearly constant for all cases (Table I). The largest reduction in acceleration occurs at the terminal point ($\tau=1$) with the relative decrease, by (6), of $3(E-2)/(2E-3) \approx 0.23$.

Comparing $\langle x_2 \rangle$ from (1) with the second term in (4), both representing numerically independent averages, we have

$$\frac{1}{2}\langle x_2 \rangle = \frac{(2E-3)H}{T^2} \quad (8)$$

or, with $T = EH/V_s$,

$$\frac{V_s^2}{H} = \frac{E^2\langle x_2 \rangle}{2(2E-3)} \approx 2660 \text{ m/s}^2 \quad (9)$$

which remains close to values deduced from all experimental records (Table I) of V_s and H . Put differently, penetration depth is practically predicted with reasonable accuracy by the relation, as shown in Fig. 9,

$$H = \frac{V_s^2}{2660} \text{ [mm]} \quad (10)$$

Finally, we make contact with cavity expansion theory by invoking the specific cavitation energy S_c defined as the energy increment required to create a unit volume. Thus, the total energy absorbed along the penetration path is

$$W = \frac{\pi}{4} D^2 H S_c \quad (11)$$

where D is projectile shank diameter. Assuming that all kinetic energy carried by the projectile equals that cavitation energy we have

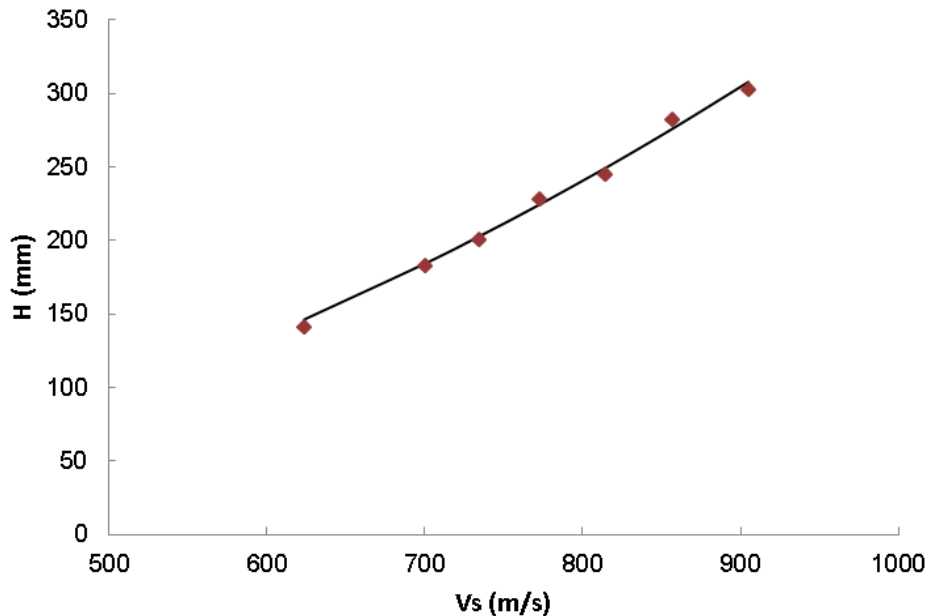


Figure 9. Final depth of penetration as function of strike velocity. Impact velocities are in the range of 624-905 m/s. Best fit curve is shown by full line.

$$\frac{\pi}{4} D^2 H S_c = \frac{1}{2} M V_s^2 \quad (12)$$

where M is projectile mass. It follows that the specific cavitation energy is given by

$$S_c = \left(\frac{2M}{\pi D^2} \right) \frac{V_s^2}{H} \quad (13)$$

For the present series of experiments we find, via (9) and data from Table I,

$$S_c \cong 290 \text{MPa} \quad (14)$$

or about 4.3 times the yield stress of polycarbonate ($Y = 65 \text{MPa}$).

Now, we will present a brief outline of the flat projectile results from Series II as they expose the scatter encountered when projectiles are not head pointed. Fig. 10 displays the penetration depth of 5 mm flat projectiles into polycarbonate as a function of time, during normal penetration, in non-dimensional plane (ξ, τ) . Table II summarizes the experimental results and the analyzed data for the flat projectiles. The value of $S_c \cong 485 \text{MPa}$ is attained via (13) using data from Table II. The high value of S_c for flat projectiles suggests that friction is non-negligible. Fig. 11 shows the penetration trajectory within the PC target which was penetrated by a flat projectile at normal impact.

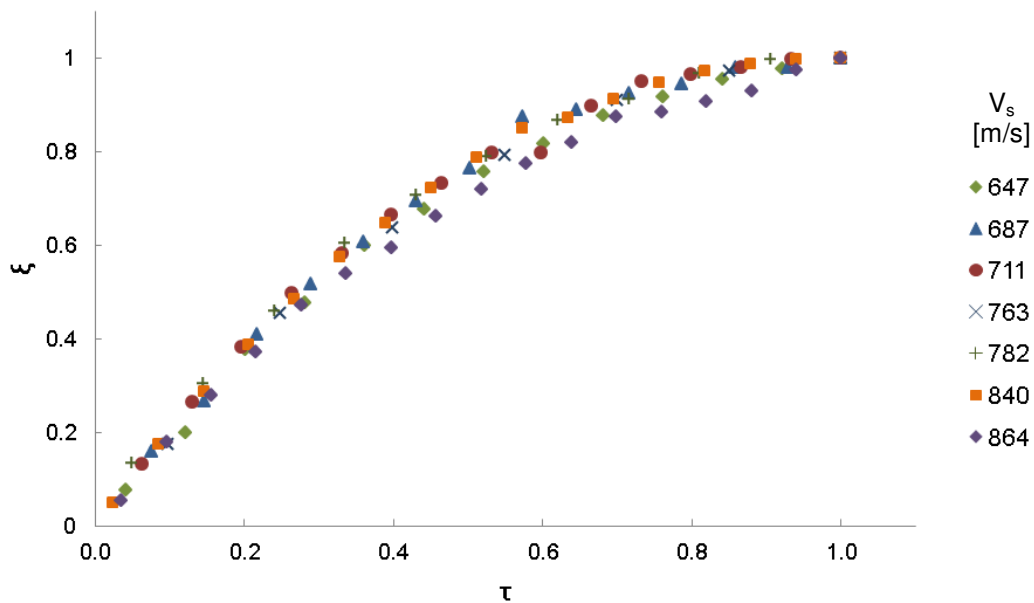


Figure 10. Normalized position ξ of flat projectile for polycarbonate as function of normalized time, τ , during normal penetration at impact velocities in the range of 647-864 m/s.

TABLE II. EXPERIMENTAL AND CALCULATED DATA FOR FLAT PROJECTILE (SERIES II)

V_s [m/s]	T [ms]	H [mm]	x_2 [$\times 10^3$ m/s ²]	x_3 [$\times 10^6$ m/s ³]	$V_s T/H$	V_s^2/H [$\times 10^3$ m/s ²]
647	0.137	44.2	5510	8136	2.01	9.47
687	0.150	50.3	4992	2706	2.05	9.38
711	0.151	53.1	5864	10515	2.02	9.52
763	0.161	60.6	5154	3159	2.03	9.61
782	0.159	59.0	6686	13650	2.11	10.36
840	0.169	70.7	5580	5166	2.01	9.98
864	0.179	79.9	6046	10629	1.94	9.34

The influence of wall function can also be assessed by comparison with the spherical cavity expansion result [11], in a Mises solid,

$$S_c = \frac{2}{3} Y \left(1 + \ln \frac{2E}{3Y} \right) \quad (15)$$

where Y is the yield stress and E the elastic modulus. For the polycarbonate material we find the value of $S_c=178$ MPa well below experimental results. Likewise, the theoretical analysis [12], for flat head projectiles, predicts that

$$S_c = Y \left(\frac{2}{3} + \ln \frac{2E}{3Y} \right) \quad (16)$$

which gives 245MPa. This value improves on the prediction of (15) but still remains below measured values for polycarbonate.



Figure 11. Deep penetration of 5 mm flat projectile in polycarbonate.

CONCLUDING REMARKS

The specific cavitation energy can be interpreted also the average resisting pressure (resisting force divided by shank cross section area) during penetration. Quasi static deep penetration experiments, reported in [7], with polycarbonate targets resulted in average pressure (after deduction of friction force) of 290MPa for flat ended punch, and 270MPa for hemispherically ended punch. By comparison, current total value which includes friction for ogive head is 290MPa, implying that the actual specific cavitation energy should be smaller.

Numerical simulation of deep penetration into polycarbonate targets with ogival projectiles are described in [8], using a rate dependent plasticity model, within the impact velocity range of 250-750m/s. With projectile mass of 7.42gr and diameter of 7.62mm calculated value of S_c are 196MPa for $V_s=250$ m/s, 251MPa (400m/s), 269MPa (500m/s), 291MPa (600m/s) and 319MPa (750m/s). The last result was supported by a single experiment. Thus, values of S_c deduced from numerical evaluations in [8] are close to our result (14) within the higher range of impact velocities.

Both studies [7]-[8] report an emergence of a damaged zone around the tunnel wall, observed as well (Figs 2-3) in our experiments. Further analysis of this phenomenon including the issue of wall friction, is given in [10]. The damaged zone can be modeled as a hackled medium with radial cracks which reduce the circumferential stress to zero.

REFERENCES

1. M.E. Backman and W. Goldsmith. 1978. "The Mechanics of Penetration of Projectiles into Targets," *Int. J. Eng. Sci.*, 16(1):1-99.
2. P. Westine. 1975. "Prediction of Transient Displacement, Velocity, and Force on Projectiles Penetrating Cohesive Soils," *J. Terramechanics.*, 12(4):149-170.
3. X. W. Chen and Q. M. Li. 2002. "Deep Penetration of a Non-Deformable Projectile with Different Geometrical Characteristics," *Int. J. Impact Eng.*, 27(6):619-637.
4. M. J. Forrestal and T. L. Warren. 2008. "Penetration Equations for Ogive-Nose Rods into Aluminum Targets," *Int. J. Impact Eng.*, 35(8):727-730.
5. Z. Rosenberg and E. Dekel. 2009. "The penetration of rigid long rods - revisited," *Int. J. Impact Eng.*, 36(4):551-564.
6. R. Masri and D. Durban. 2009. "Deep Penetration Analysis with Dynamic Cylindrical Cavitation Fields," *Int. J. Impact Eng.*, 36(6):830-841.
7. S. C. Wright and Y. Huang and N. A. Fleck. 1992. "Deep Penetration of Polycarbonate by a Cylindrical Punch," *Mech. Mater.*, 13(4):277-284.
8. A. Dorogoy, D. Rittel and A. Brill. 2011. "Experimentation and modeling of inclined ballistic impact in thick polycarbonate plates," *Int. J. Impact Eng.*, 38(10):804-814.
9. S. Bless. 2012. "Using Depth-of-Penetration Tests to Design Transparent Armor," *Experimental Mechanics*, in press.
10. A. Weiss. M.Sc. Research Thesis, in preparation, Technion.
11. R. Hill. 1950. *The Mathematical Theory of Plasticity*. Oxford University Press.
12. A. Tate. 1986. "Long Rod Penetration Mechanics - Part I. The Flow Field Model for High Speed Long Rod Penetration," *Int. Mech. Sci.*, 28(8):535-548.